

Resolving singular forces in cavity flow: Multiscale modeling from atoms to millimeters

Xiaobo Nie¹, Mark. O. Robbins^{1,2}, and Shiyi Chen^{2,3}

¹*Department of Physics and Astronomy, The Johns Hopkins University, Baltimore, MD 21218*

²*Department of Mechanical Engineering, The Johns Hopkins University, Baltimore, MD 21218*

³*CCSE and SKLTCS, Peking University, Beijing, China*

A multiscale approach for fluid flow is developed that retains an atomistic description in key regions. The method is applied to a classic problem where all scales contribute: The force on a moving wall bounding a fluid-filled cavity. Continuum equations predict an infinite force due to stress singularities. Following the stress over more than six decades in length in systems with characteristic scales of millimeters and milliseconds allows us to resolve the singularities and determine the force for the first time. The speedup over pure atomistic calculations is more than fourteen orders of magnitude. We find a universal dependence on the macroscopic Reynolds number, and large atomistic effects that depend on wall velocity and interactions.

PACS: 47.11.+j, 68.08.-p, 89.75.-k, 81.07.Nb

Processes that span a wide range of length scales pose profound theoretical challenges [1, 2]. The different length scales must be followed with different time resolutions and may require qualitatively different descriptions of matter. For example, discrete atomistic effects may be important in regions of high stress or rapid spatial variation, while other regions are most naturally and efficiently modeled as a continuous medium. Important examples of such problems include adhesion and friction [3, 4], deformation of crystalline solids [5, 6], distribution and flow of charges at biological interfaces, flow near solid surfaces [7], and the many cases where continuum equations lead to singularities.

Several innovative paradigms for bridging between atomistic and macroscopic scales have been proposed in recent years, and tested against purely atomistic simulations in small idealized systems [8, 9, 10, 11, 12, 13, 14, 15]. A few have been applied to specific problems with a large range of scales. Notable examples include calculations of crack propagation in silicon that include electronic structure near the crack tip [16], and calculations of indentation with the quasicontinuum method [17]. However, these applications have only reached micrometer length and nanosecond time scales, and the main effect of large scales is to provide appropriate boundary conditions for the atomistic region.

In this paper we consider a classic problem in fluid mechanics where all length scales contribute equally: the force on a moving boundary of a fluid filled cavity. Using different spatial and temporal resolutions in different regions allows us to treat cavities with dimensions of order millimeters and characteristic times of tens of milliseconds. Our multiscale approach accelerates the calculation by more than fourteen orders of magnitude compared to brute force atomistic simulations. Spanning many decades in length scale allows us to build a simple scaling relation for the total force F that captures both atomistic effects and the influence of the only parameter in continuum theory, Reynolds number.

Cavity flow has intrigued scientists because of singu-

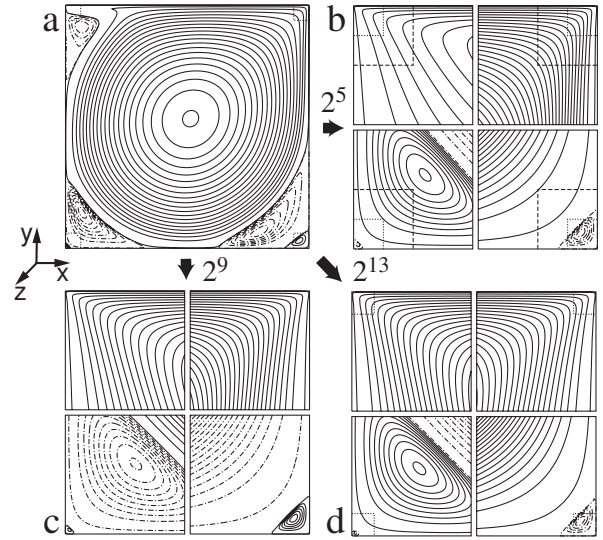


FIG. 1: Geometry and streamlines for cavity flow at $Re \equiv \rho UL/\mu = 6400$. a) The square cavity has edge $L = 10^6\sigma \sim 0.3\text{mm}$ in the $x-y$ plane, the top wall moves to the right at speed U , the flow is independent of z , and the natural time scale to reach steady state flow is $\sim 40\text{ms}$. Solid (dash-dotted) streamlines indicate clockwise (counter-clockwise) flow. In (b-d), flow near each corner is magnified by the indicated factor. The coupling of different resolutions is illustrated in b. The coarser solution provides boundary conditions along the outer boundary of the finer grid (dashed lines) and obtains them along the dotted lines. In (d), dotted lines indicate the boundaries of the $\sim 12\sigma$ wide regions that are treated atomistically.

larities that can not be resolved by purely continuum methods. Figure 1a illustrates the cavity geometry. The top wall is displaced to the right at fixed velocity \mathbf{U} and the other walls are stationary. The traditional continuum approach to this problem uses the Navier-Stokes (NS) equations and no-slip boundary conditions at the

walls [18, 19, 20]. The no-slip condition requires that the fluid velocity \mathbf{u} vanishes near static walls, and equals \mathbf{U} at the moving wall. The discontinuity in boundary condition at corners between moving and fixed walls causes the stress to diverge as the inverse of the distance from the corner, r . The total force on the wall is the integral of the stress, and diverges logarithmically in continuum theory.

Koplik and Banavar pioneered the use of molecular dynamics (MD) to study the singularities in cavity flow [21]. They observed a breakdown of the no-slip boundary condition within atomic distances from the corner, and a corresponding saturation of the stress. Similar effects cut off stress singularities in the closely related problem of spreading fluids [22, 23]. Koplik and Banavar's purely atomistic approach limited the cavity length to $L = 17\sigma$, where $\sigma \sim 0.3\text{nm}$ corresponds to a molecular diameter. We recently extended L to $250\sigma \sim 75\text{nm}$ using a hybrid method that treated singular regions atomistically and the remainder of the cavity as a continuum. This approach allowed us to analyze the breakdown of the continuum boundary conditions over a wider range of U , and to determine its microscopic origins [24]. The stress deviates from the singular continuum solution for $r < S(U)$. At low U , the intrinsic discreteness of atomic fluids leads to $S \sim \sigma$. At large U , the interfacial stress is high enough to produce non-Newtonian effects [7], and S rises linearly with U .

To study cavities with millimeter scale dimensions, two major improvements must be made on previous work. The first is to vary the resolution in the continuum region to efficiently describe the rapid increase in velocity gradients near the singular corners. We chose to do this using a local refinement approach [25]. The second is to span the wide range of time scales associated with different spatial resolutions. While the motion of atoms near the corner must be followed with time steps of order 10^{-14}s , the time for flows to equilibrate on millimeter scales, $\sim 100L/U$, may be of order seconds. To overcome this obstacle we use the optimum time step to obtain the steady state flow at each spatial scale, and then enforce self-consistency between scales.

The details of our approach and a sample flow field are illustrated in Fig. 1. At the continuum scale the flow is independent of z , and satisfies the NS equations with viscosity μ , fixed density ρ , and no-slip boundary conditions. At each scale the NS equations are discretized on a square grid of cells with width h , and the steady state flow is obtained using an artificial compressibility method [26] with time step of $1/4 - 1/2 h/U$. On the coarsest scale $h = L/256$. This resolution is inadequate near the corners, where h is decreased by successive factors of two using an iterative refinement scheme.

At each stage of the iteration, solutions at two resolutions provide boundary conditions for each other. The geometry is illustrated in Fig. 1b. Both resolutions use a 64 by 64 array of square cells. The finer grid lies in the inner quarter of the coarse grid (dashed lines), and receives

boundary conditions on its outer edge. It in turn provides boundary conditions for the coarser grid along the dotted lines. The overlap region between dashed and dotted lines prevents discontinuities due to sudden changes in resolution [9, 10, 12].

This refinement scheme is iterated until the overlap region reaches nanometer scales. There the finest resolution results are obtained from MD simulations that can be extended all the way into the corner (Fig. 1d). At the outer edge of the MD region the mean atomic velocity is constrained to follow the finest continuum solution ($h = 0.95\sigma$) and particles are added or removed to match the continuum flux [9, 24]. Average MD velocities provide boundary conditions for the continuum solution along an inner square whose edge is 6 cells long. A global steady state solution is obtained by iterating from coarsest to finest scale and then back to the coarsest scale until all boundary conditions are consistent. This typically requires ten to twenty iterations, depending on the desired accuracy.

To obtain a smooth solution, the continuum model must accurately describe the atomistic behavior at the outer boundary of the MD region. This requires consistent choices of μ and molecular interactions. Following previous work [21, 24], we consider fluid atoms of mass m interacting with a Lennard-Jones (LJ) potential of characteristic energy ϵ and diameter σ . The potential is truncated at $r_c = 2.2\sigma$, and the mass density $\rho = 0.81m\sigma^{-3}$. The geometry and interactions of the crystalline walls are chosen to produce a no-slip boundary condition far from the corner [24]. Discrete wall atoms are on the sites of a (111) surface of an fcc crystal of lattice constant 1.204σ and interact with the fluid with a LJ potential with energy $\epsilon_{wf} = 0.95\epsilon$.

Within the MD region, the motion of particles is fully three-dimensional. However the mean flow velocities are independent of z , and periodic boundary conditions with period L_z are applied in this direction. The equations of motion are integrated using the Verlet scheme with time step $\Delta t_{MD} = 0.005t_{LJ}$, where $t_{LJ} \equiv (m\sigma^2/\epsilon)^{1/2}$ is the characteristic time of the LJ potential. A constant temperature $k_B T = 1.1\epsilon$ is maintained by applying a Langevin thermostat [27] with damping rate $\Gamma = 1t_{LJ}^{-1}$ in the z direction. The dynamic viscosity [10] of the LJ fluid $\mu = 2.14\epsilon t_{LJ}\sigma^{-3}$ is used in the NS equations.

Two lengths characterize transitions in flow behavior near each corner. Inertial effects are significant for $r > r_I \equiv \mu/\rho U$, while deviations from continuum behavior occur for $r < S(U)$. At intermediate scales our results follow the analytic solution for Stokes (non-inertial) flow [18]. Near the top corners the streamlines are scale invariant because \mathbf{u} only depends on the angle relative to the moving wall. The stress diverges as $1/r$ since \mathbf{u} changes by U over a length of order r . A series of counter-rotating vortices forms near the bottom corners. The change in scale between panels in Fig. 1 was chosen to illustrate the predicted self-similarity under $r \rightarrow r/16.4$ and a change in direction of rotation [19, 28]. The vortices are cut off

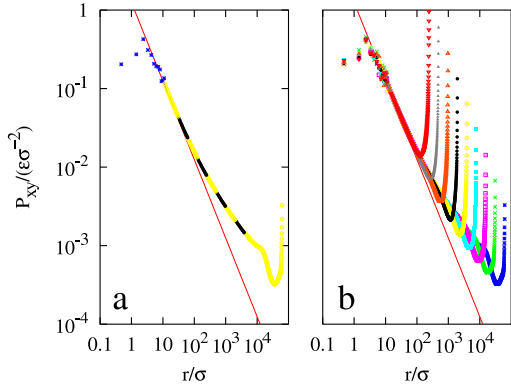


FIG. 2: Shear stress as a function of distance r from the upper left corner for $U = 0.27\sigma/t_{LJ}$. Qualitatively similar scaling occurs near the upper-right corner. In (a) $Re = 6400$, $L = 6.25 \times 10^4\sigma$, $r_I = 9.8\sigma$, $S \approx 2.2\sigma$, lines of alternating color indicate continuum results from successive resolutions, and asterisks show MD results. Results for $Re = 25$ to 6400 obtained by increasing L by factors of two are compared in (b).

at $S(0) \sim \sigma$ by atomistic effects, and this is responsible for the small deviation between panels c and d.

Fig. 2(a) shows a plot of the shear stress τ along the moving wall at Reynolds number $Re \equiv \rho UL/\mu = 6400$ as a function of distance r from the upper-left corner. Alternating colors are used for data from different resolutions to illustrate the smooth matching. The asterisks are from the force per unit area on wall atoms in the atomistic region. At intermediate scales, the stress follows the divergence predicted by the Stokes solution $\tau = (4\pi)/(\pi^2 - 4)(\mu U)/r$ (straight line). At large scales the stress decays more slowly than $1/r$, and at $r < S \approx 2.2\sigma$ the stress singularity is cutoff by atomistic effects. Fig. 2(b) shows that changing Re by increasing L only changes the flow in the outer region. At scales of order $L/2$ the other corners become important, but for $r \ll L/2$ all results fall onto a common curve. This shows that S is independent of L and only depends on U and atomic properties.

The total shear force on the moving wall is an integral of the shear stress along it. Fig. 3 shows the force per unit length along the z -direction, F , as a function of Re . If the Stokes solution applied, each factor of two in length scale would contribute the same force and the total would diverge. This divergence is cutoff by atomistic effects at $r < S$ but inertial effects enhance the force from $r > r_I$. To determine F , one must resolve the inertial effects between r_I and $L = Re r_I$ as well as the atomistic behavior at the corner. Our approach enables us to span this wide range of scales ($> 10^5$) for the first time.

If atomistic effects were not important, the dimensionless force on the wall $f \equiv F/\mu U$ would only depend on

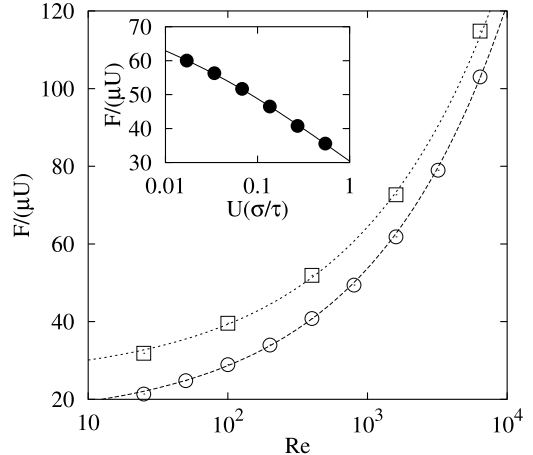


FIG. 3: Dimensionless force per unit length on the sliding wall $F/\mu U$ as a function of Reynolds number $Re = \mu UL/\rho$. Results for $U = 0.27\sigma/t_{LJ}$ (circles) and $U = 0.068\sigma/t_{LJ}$ (squares) follow Eq. 1 (dashed lines) with $S = 2.2$ and 0.55 respectively. The inset compares the calculated force vs. velocity at $Re = 400$ (circles) to Eq. 1 (line).

Re . However, Fig. 3 shows that changing U at fixed Re produces large shifts in f . A complete description of f can be obtained by considering the separate contributions, f_i , of the three scaling regimes in the stress shown in Fig. 2. They are well-separated as long as $Re = L/r_I \gg 1$ and the Reynolds number at molecular scales $Re_m \approx S/r_I \ll 1$.

The dependence on Re comes entirely from the outer region $r > r_I$, which is why curves for different U in Fig. 3 are related by a constant shift. As shown in Fig. 2(b), increasing Re extends the range of the inertial tail that contributes to the dimensionless force, causing $f_3(Re)$ to rise with Re . For $Re > 10$ our numerical results are well described by $f_3 = a + bRe^\alpha$ with $a = 3.85$, $b = 1.98$ and $\alpha = 0.434$.

In the inner region near each corner, $r < S$, the stress is determined entirely by U and atomic properties, such as t_{LJ} , σ , ρ , and wall geometry (Fig. 2(b)). For fixed interactions, we can write the contribution from this regime as $f_1(U t_{LJ}/\sigma)$. In fact we find f_1 has a constant value of about 4.3. The reason is that the range of integration grows linearly with S while the stress scales inversely with S . Indeed assuming the stress for $r < S$ is equal to the Stokes stress at S yields $f_1 = 8\pi/(\pi^2 - 4) \approx 4.28$, which is consistent with the numerical results. The value of f_1 is as much as 20% of the total wall force in Fig. 3, yet it comes from an inner region that is never larger than a few molecular diameters. This is clear evidence of the direct effect of atomic scale behavior on the macroscopic force.

In the intermediate region, $S < r < r_I$, the Stokes solution applies, and can be integrated to give $f_2(r_I/S) =$

$8\pi/(\pi^2 - 4)\ln(r_I/S)$. This term is responsible for the velocity dependence in the total dimensionless force:

$$\frac{F}{\mu U} = f_1 + \frac{8\pi}{\pi^2 - 4} \ln(r_I/S) + a + bRe^\alpha . \quad (1)$$

The ratio S/r_I reflects the range at which atomistic effects cut off the Stokes region, and decreases as U decreases. The inset to Fig. 3 shows that numerical results for the velocity dependence of F are consistent with $S = S_0 + kUt_{LJ}$ with $S_0 = 0.3\sigma$ and $k = 7$. This form for S is consistent with our previous studies [24], which showed S approached a constant of atomic scale at low velocities and rose linearly with U at high velocities due to non-Newtonian effects.

Our multiscale method has allowed us to span the wide range of length scales ($> 10^5$) that contribute to the drag force on the moving wall of an ideal cavity, and to extract a simple and accurate physical description (Eq. 1) of the important contributions from each scale. We have used it to treat cavities with dimensions of order millimeters

and natural time scales approaching seconds, and the approach is readily extended to still larger scales. Its major limitation is that it assumes a steady state solution, while cavity flow becomes turbulent at $Re > 8000$ [29]. It may be possible to extend simulations into the turbulent regime using ideas like the ‘‘equation-free’’ approach of Kevrekidis et al.[15]. Turbulent fluctuations occur on the longer time scales associated with coarser resolutions, and the finer scales can be iterated to a quasistatic state that follows the coarse solution. This would allow calculations with the same coarse time step that is used in a completely continuum description, while retaining the crucial atomic detail. We hope that our work encourages such efforts, as well as applications to other important multiscale problems such as contact-line motion and contact mechanics.

Acknowledgments. This material is based upon work supported by the U.S. National Science Foundation under Grant No. CMS-0103408 and the Digital Laboratory for Multiscale Science.

-
- [1] J. Glimm and D. H. Sharp, SIAM News **30** (1997).
 [2] T. Y. Hou, Int. J. Numer. Meth. Fluids **47**, 707 (2005).
 [3] M. Urbakh, J. Klafter, D. Gourdon, and J. Israelachvili, Nature **430**, 525 (2004).
 [4] B. Luan and M. O. Robbins, Nature **435**, 929 (2005).
 [5] M. D. Uchic, D. M. Dimiduk, J. N. Florando, and W. D. Nix, Science **305**, 986 (2004).
 [6] J. Weiss and D. Marsan, Science **299**, 89 (2002).
 [7] P. A. Thompson and S. M. Troian, Nature **389**, 360 (1997).
 [8] J. Li, D. Liao, and S. Yip, Phys. Rev. E **57**, 7259 (1998).
 [9] X. B. Nie, S. Y. Chen, W. N. E, and M. O. Robbins, J. Fluid Mech. **500**, 55 (2004).
 [10] S. T. O’Connell and P. A. Thompson, Phys. Rev. E **52**, R5792 (1995).
 [11] N. G. Hadjiconstantinou and A. T. Patera, Inter. J. Mod. Phys. C **8**, 967 (1997).
 [12] E. G. Flekkoy, G. Wagner, and J. Feder, Europhys. Lett. **52**, 271 (2000).
 [13] V. B. Shenoy, R. Miller, E. B. Tadmor, R. Phillips, and M. Ortiz, Phys. Rev. Lett. **80**, 742 (1998).
 [14] W. Q. Ren and W. N. E, J. Comp. Phys. **204**, 1 (2005).
 [15] I. G. Kevrekidis, C. W. Gear, and G. Hummer, AIChE J. **50**, 1349 (2004).
 [16] J. Q. Broughton, F. F. Abraham, N. Bernstein, and E. Kaxiras, Phys. Rev. B **60**, 2391 (1999).
 [17] J. Knap and M. Ortiz, Phys. Rev. Lett. **90**, 226102 (2003).
 [18] G. K. Batchelor, *An Introduction to Fluid Dynamics* (Cambridge, Cambridge, 1967).
 [19] F. Pan and A. Acrivos, J. Fluid Mech. **28**, 643 (1967).
 [20] U. Ghia, K. N. Ghia, and C. Y. Shin, J. Comput. Phys. **48**, 387 (1982).
 [21] J. Koplik and J. R. Banavar, Phys. Fluids **7**, 3118 (1995).
 [22] J. Koplik, J. R. Banavar, and J. F. Willemsen, Phys. Rev. Lett. **60**, 1282 (1988).
 [23] P. A. Thompson and M. O. Robbins, Phys. Rev. Lett. **63**, 766 (1989).
 [24] X. B. Nie, S. Y. Chen, and M. O. Robbins, Phys. Fluids **16**, 3579 (2004).
 [25] S. F. McCormick, *Multilevel Adaptive Methods for Partial Differential Equations* (SIAM, Philadelphia, 1989).
 [26] R. Peyret and T. D. Taylor, *Computational Methods for Fluid Flow* (Springer-Verlag, New York, 1983).
 [27] G. S. Grest and K. Kremer, Phys. Rev. A **33**, 3628 (1986).
 [28] H. K. Moffatt, J. Fluid Mech. **18**, 1 (1964).
 [29] W. Cazemier, R. W. C. P. Verstappen, and A. E. P. Veldman, Phys. Fluids **10**, 1685 (1998).